

**Notice to Data Users:**  
**The documentation for this data set was provided solely by the Principal Investigator(s) and was not further developed, thoroughly reviewed, or edited by NSIDC. Thus, support for this data set may be limited.**

## **Daily Global Land Surface Parameters Derived from AMSR-E**

### **Data Summary:**

This data set contains satellite-retrieved geophysical parameter files generated from the Advanced Microwave Scanning Radiometer - Earth Observing System (AMSR-E) instrument on the National Aeronautics and Space Administration (NASA) Aqua satellite. The daily parameter retrievals extend from 19 June 2002 to 27 September 2011 and include daily air temperature minima and maxima (ta) at approximately 2 m height; fractional cover of open water on land (fw); vegetation canopy microwave transmittance (tc); surface soil moisture (mv) at  $\leq 2$  cm soil depth; and integrated water vapor content of the intervening atmosphere (V) for the total column. The global retrievals were derived over land for non-precipitating, non-snow, and non-ice covered conditions. The primary input data were daily AMSR-E dual polarized multi-frequency, ascending and descending overpass brightness temperature data. The total volume for this data set is approximately seven gigabytes. Data are provided in zipped binary files and are available via FTP. The AMSR-E brightness temperature data were obtained in the global 25-km EASE-Grid projection from the National Snow and Ice Data Center (NSIDC), (Knowles et al. [2006]). NSIDC uses the AMSR-E/Aqua L2A Global Swath Spatially-Resampled Brightness Temperatures (AE\_L2A) swath data product, which represents all frequencies resampled to a common spatial resolution, to produce these grids (Ashcroft and Wentz [1999]). This results in some degree of spatial smoothing due to gridding and re-projection of the AMSR-E L2A brightness temperature inputs to a consistent 25-km resolution grid. Detailed descriptions of the algorithms and calibration/validation of associated parameter retrievals are provided by Jones et al. [2009, 2010]. This data set was produced at the University of Montana and the Jet Propulsion Laboratory (JPL) under contract to the National Aeronautics and Space Administration (NASA).

### **Citing These Data:**

These data are offered free of charge. You may use these data freely, provided that you cite NSIDC as the source, and provide an acknowledgment in any published papers.

Jones, Lucas A. and John S. Kimball. 2010, updated 2012. *Daily Global Land Surface Parameters Derived from AMSR-E*. Boulder, Colorado USA: NASA DAAC at the National Snow and Ice Data Center.

### Literature Citation

We kindly request that you acknowledge the author(s) of this data set by referencing the following peer-reviewed publication.

Jones, L. A., C. R. Ferguson, J. S. Kimball, K. Zhang, S. Chan, K. C. McDonald, E. G. Njoku, and E. F. Wood. 2010. Satellite Microwave Remote Sensing of Daily Land Surface Air Temperature Minima and Maxima From AMSR-E. *IEEE Journal of Selected Topics in Applied Earth Observations and Remote Sensing* 3(1): 111-123. <http://dx.doi.org/10.1109/JSTARS.2010.2041530>.

# Version 1.2, Update 1

## Contact Information:

Lucas A. Jones and John S. Kimball  
Numerical Terradynamic Simulation Group (NTSG)  
The University of Montana  
Missoula MT, 59812  
Email: [lucas@ntsg.umt.edu](mailto:lucas@ntsg.umt.edu); [johnk@ntsg.umt.edu](mailto:johnk@ntsg.umt.edu)  
URL: <http://ntsg.umt.edu>  
Document last updated: 4-23-12

## Contents

I. Data Description .....	1
II. Data Format .....	2
III. File naming convention .....	3
IV. Manifest .....	3
V. Ancillary Code and Data (\ <code>ancil</code> ) .....	4
VI. Mapping and Visualization .....	4
VII. Example Figures .....	5
VIII. Notes on Accuracy .....	7
IX. Additional Methods .....	8
X. Version and Update List .....	10
XI. References .....	11

## I. Data Description

This directory contains satellite retrieved geophysical land parameter files generated from the Advanced Microwave Scanning Radiometer on EOS Aqua (AMSR-E). The daily retrievals extend from June 19 (day 170), 2002 to September 27 (day 270), 2011 and include daily air temperature minima and maxima ( $ta$ , ~2 m height), fractional cover of open water on land ( $fw$ ), vegetation canopy microwave transmittance ( $tc$ ), surface soil moisture ( $mv$ ,  $\leq 2$  cm soil depth)

and integrated water vapor content of the atmosphere ( $V$ , total column). The global retrievals are derived over land for non-precipitating, non-snow-covered, and non-ice covered conditions. Data pre-screening was performed with an external temporal change classification of frozen land areas derived from AMSR-E 36 GHz V-pol. (ascending and descending) brightness temperature timeseries (algorithm from Kim *et al.* 2011). Other employed pre-screening classifications rely on input brightness temperature indices (Jones *et al.* 2010; Njoku *et al.* 2005; Grody 1988; also see Section IX.). After pre-screening, the primary algorithm inputs are daily AMSR-E dual polarized multi-frequency, ascending and descending overpass brightness temperature ( $Tb$ ) data (version 3) obtained in global 25-km EASE-Grid format from the National Snow and Ice Data Center (NSIDC) on 2/01/11 (Knowles *et al.* 2006). NSIDC produces these grids using the AE\_L2A swath data product (version 3), in which all frequencies are re-sampled to a common spatial resolution (Ashcroft and Wentz 1999). The gridding procedures result in some degree of spatial smoothing due to re-sampling and re-projecting of the AMSR-E L2A brightness temperature inputs to a consistent 25-km grid. Detailed descriptions of the parameter retrieval algorithms are provided by Jones *et al.* (2009, 2010) and algorithm development is ongoing. Further validation is discussed in Jones *et al.* 2011 and Yi *et al.* 2011. These data were produced at the University of Montana and the Jet Propulsion Laboratory under contract to the National Aeronautics and Space Administration (NASA). The data are appropriate for global change-related assessment of land-atmosphere water, energy and carbon cycle interactions.

Changes from Version 1.1 (original release) to 1.2 (current version) include correction of a gridding error in the land-water mask and an additional flag indicating simultaneous occurrence of 6.9 and 10.7 GHz RFI. A version list and further details on changes are given in Section X.

Although extensive quality checking has been completed, these are research data. The user is responsible for quality checking and should be aware that spurious values may exist. Authors hold no responsibility for conclusions drawn from spurious data. We appreciate constructive and well-documented feedback to help make these data more useful. Questions and feedback should be sent to Lucas Jones (lucas@ntsg.umt.edu).

## II. Data Format

Each retrieval file contains a 209091 element 1D binary array representing the global land area defined as containing <50% open water and <50% permanent ice according to the MODIS MOD12Q1 v4 IGBP 1-km land cover classification which was binned to the 25-km global EASE grid. The purpose of the 1D array format is to avoid allocating memory to placeholder values over the oceans. The full 586×1383 global EASE grid can be created from the 1D data arrays using provided ancillary row and column files (See Section V.). Each year's directory contains separate subdirectories for each retrieved parameter in the following data types: 1-byte integer; 2-byte integer; 4-byte integer. See below for more detailed metadata and documentation.

### III. File naming convention

{parameter}\_ {year} {day of year (1:365)} {overpass (A or D)}.bin

The parameter prefix strings are listed in the manifest (Section IV.). The year string contains four digits. The day-of-year is the day since January 1 of the current year (three digits). December 31 (day 366) is omitted from all leap years. The overpass character is either A for ascending (afternoon; P.M.) or D for descending (morning; A. M.).

### IV. Manifest

**flags** (1-byte) Flags for screening missing Tb, snow cover, rain, and radio frequency interference (RFI) in the 6.9, 10.7, and 18.7 GHz channels. The flags are hierarchical; that is a flag is assigned once a condition is met even if several other conditions lower on the hierarchy (higher flag numbers) were also present. For example if flag = 2 snow is present, but rain, RFI, etc. may also be present and if flag = 3 rain was detected and snow was not detected, and RFI may be also be present.

0 = Good data	(used in the retrieval)
1 = Missing Tb	(Tb not collected by the AMSR-E instrument)
2 = Freeze-Thaw	(external frozen land surface classification)
3 = Snow/Ice Cover	(scattering from snow, sea ice, and glacial ice)
4 = Precipitation	(scattering from precipitation)
5 = 18.7 GHz RFI	(RFI in 18.7 GHz H polarization)
6 = 6.9 and 10.7 GHz RFI	(RFI in both channels)
7 = 10.7 GHz RFI	(RFI in 10.7 GHz H or V polarization)
8 = 6.9 GHz RFI	(RFI in 6.9 GHz H or V polarization)

**ta** (2-bytes) Multiply by 1e-1 to obtain surface air temperature in Kelvin. Daily temperature minima (maxima) generally occurs during the morning descending pass, 'D' (afternoon ascending pass, 'A'). Occasionally, temperatures from pass 'A' may be higher than those from pass 'D'. Valid range: 240- 340 K.

**V** (2-bytes) Multiply by 1e-1 to obtain vertically integrated atmospheric water vapor in mm. Valid range: 0-80 mm.

**fw** (2-bytes) Multiply by 1e-4 to obtain open water fraction (dimensionless). Valid range: 0-1.

- fws**m (2-bytes) Multiply by  $1e-4$  to obtain open water fraction (dimensionless) smoothed with 30-day moving median filter. Valid range: 0-1.
  
- tc** (2-bytes) Multiply by  $1e-4$  to obtain vegetation opacity (dimensionless) for the specified frequency (postfix 6, 10, and 18 represent 6.9, 10.7, and 18.7 GHz, respectively). Vegetation optical depth is calculated as  $-\log(tc)$ . The data were smoothed using a 30-day moving median filter. Valid range: 0-1.
  
- mv** (2-bytes) Multiply by  $1e-4$  to obtain surface (0-2 cm) volumetric soil moisture. Valid range: 0-1, but usually  $\leq 0.5$ . See the “RFI mitigation” section below.

## V. Ancillary Code and Data (`\ancil`)

The files `globland_r` and `globland_c` (2-byte integers) correspond to the respective rows and columns of the 25-km global EASE grid. The MATLAB function `mkgrid.m` uses these to recreate the global EASE grid matrix for viewing images and maps; however, the code is simple and can easily be adapted to another script or programming language. The files `MLLATLSB` and `MLLONLSB` (4-byte integers) contain latitude and longitude (multiply by  $1e-5$ ) for geo-locating the full global EASE grid matrix ( $586 \times 1383$ ). The directory `\ancil\lc` contains files `MOD12Q1.2003001_{type}_ease.dat` (2-byte integers) with the count of 1-km MODIS of each IGBP landcover type within each global EASE grid cell ( $586 \times 1383$ ). Also in this directory is a file `MOD12Q1.2003001_cnt_ease.dat` (4-byte integers) containing the total number of 1-km MODIS grid cells falling into each 25-km EASE grid cell. To calculate the percentage of each landcover type in each EASE grid cell divide the count for each type by the total count and multiply by 100.

## VI. Mapping and Visualization

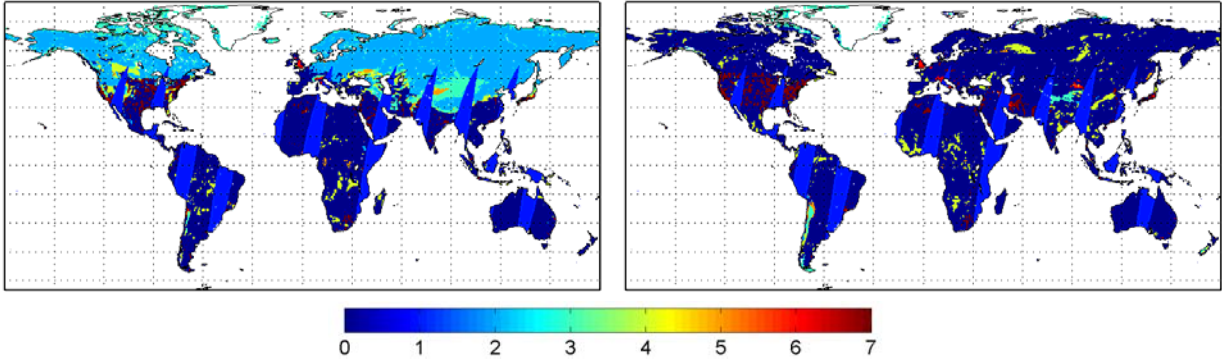
The full global 25-km EASE grid can be re-created using the provided `mkgrid_global.m` MATLAB function. If you do not use MATLAB, this simple routine can be easily modified into the programming language of your choice. Latitude and longitude (`MLLATLSB` and `MLLONLSB`) files are provided for geo-locating the global EASE grid matrix by the National Snow and Ice Data Center (NSIDC). You can visualize the data using the example MATLAB file, `ExampleMaps.m` (included).

## VII. Example Figures

### Flags

Jan. 1, 2003 (Descending)

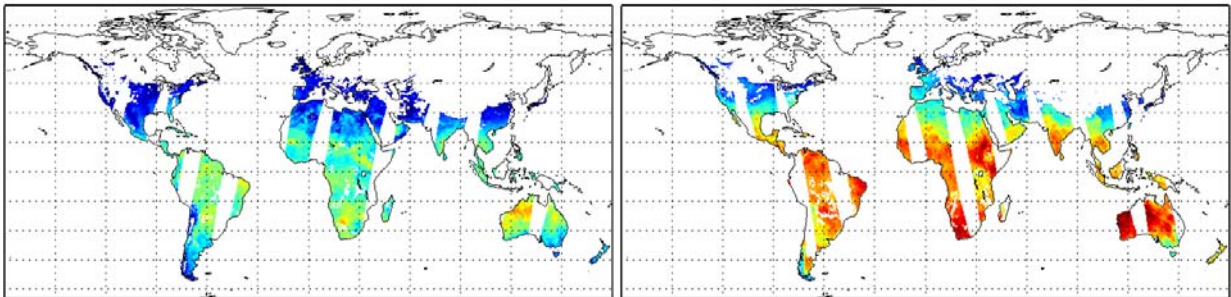
Sept. 5, 2003 (Descending)



### Min./Max. Temperature [deg. C]

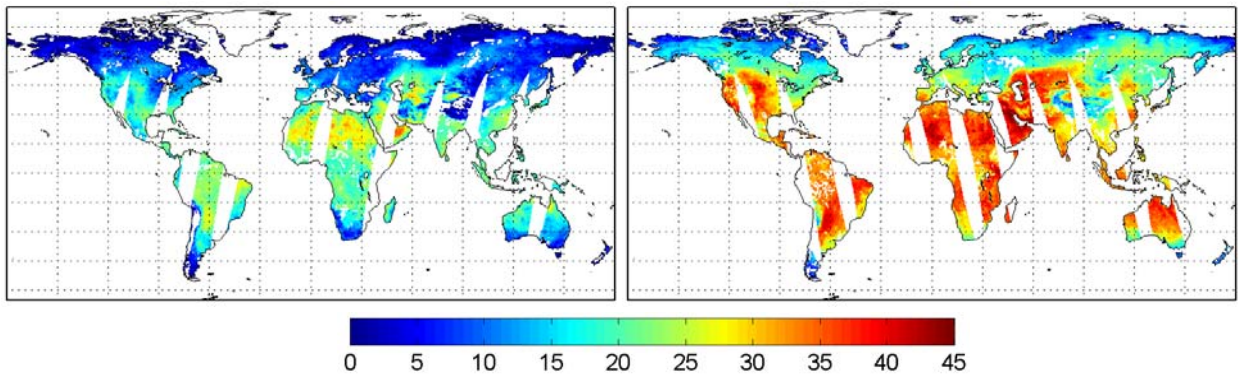
Jan. 1, 2003 (Descending)

Jan. 1, 2003 (Ascending)



Sept. 5, 2003 (Descending)

Sept. 5, 2003 (Ascending)

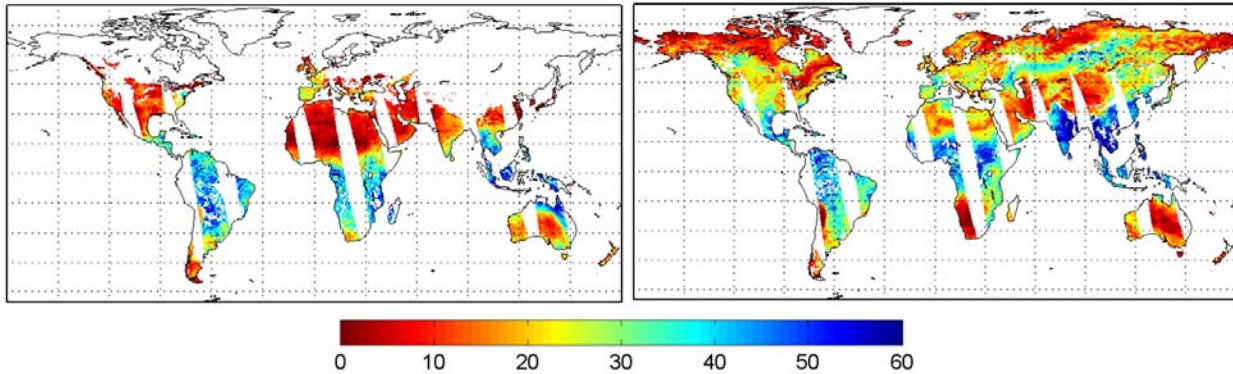




## Atmospheric Water Vapor [mm]

Jan. 1, 2003 (Ascending)

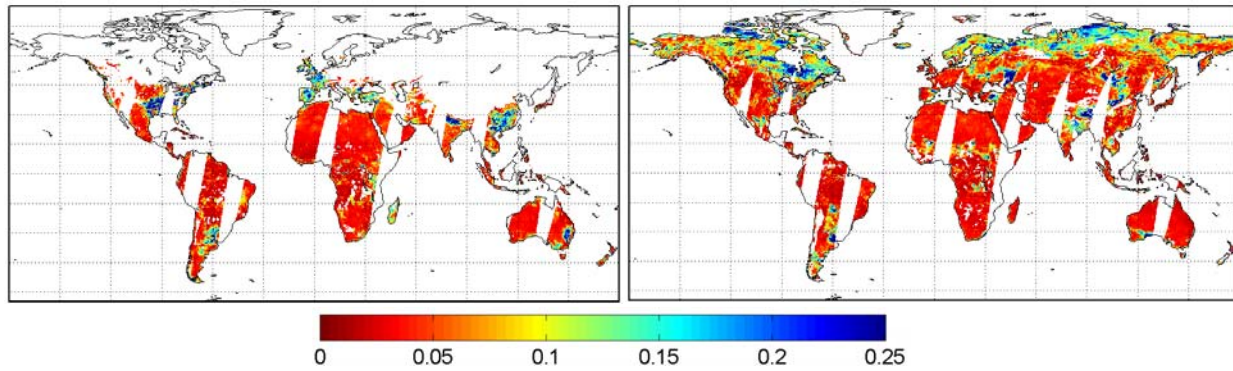
Sept. 5, 2003 (Ascending)



## Soil Moisture<sup>1</sup> [vol.]

Jan. 1, 2003 (Descending)

Sept. 5, 2003 (Descending)

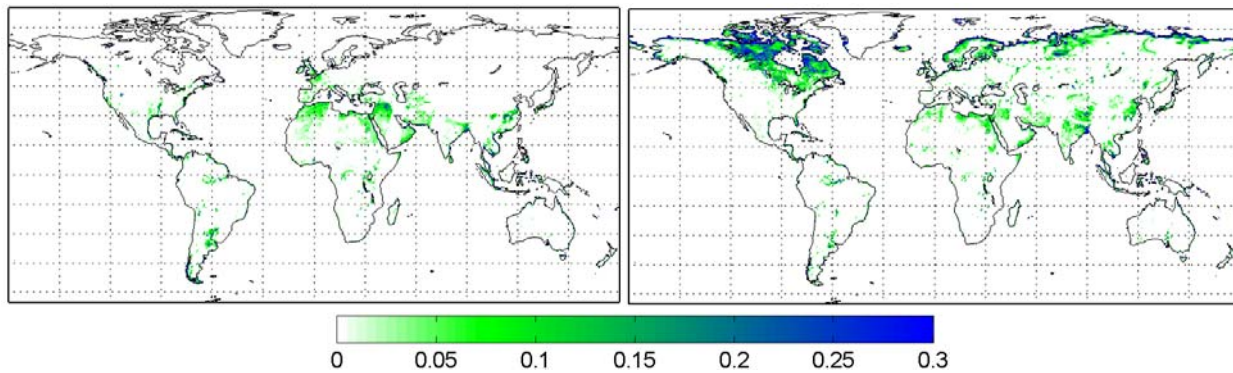


<sup>1</sup>Shown are all non-flagged data. Users should additionally screen for dense vegetation using the provided vegetation optical depth data. For example: the Amazon appears dry, counter to expectation, because the radiometer can not “see” through the forest canopy.

## Open Water Fraction [dim.]

Jan. 1, 2003 (Descending)

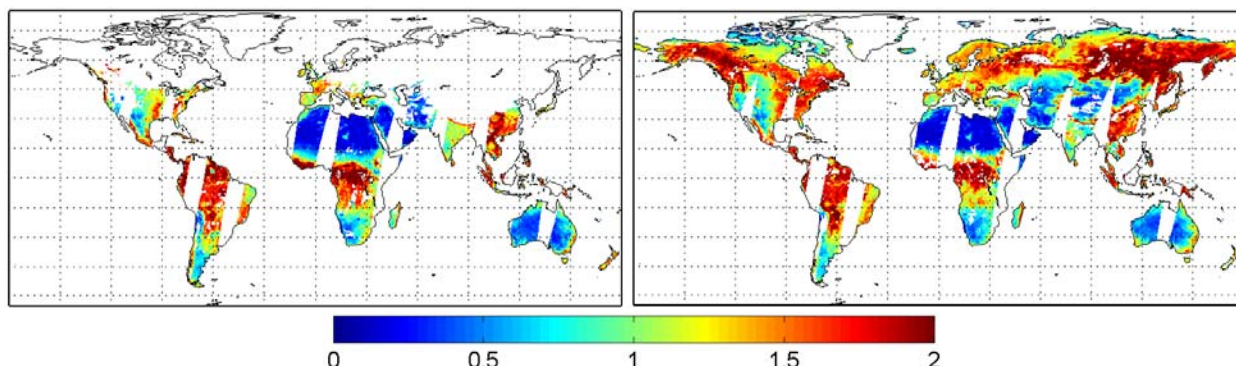
Sept. 5, 2003 (Descending)



## Vegetation Optical Depth 10.7 GHz [dim.]

Jan. 1, 2003 (Descending)

Sept. 5, 2003 (Descending)



### VIII. Notes on Accuracy

**ta:** The temperature data have been extensively compared to the WMO surface station summary of the day and AIRS/AMSU surface air temperature retrievals for the Northern Hemisphere (Jones *et al.* [2010]). The accuracy (RMSE) of this product is expected to be 1 – 4 K for the majority of surface stations in vegetated areas. Sparsely vegetated or mountainous areas may contain additional biases relative to surface stations. Biases result from emissivity effects which dominate in desert regions and are not accounted for in the retrieval algorithm. For example, this can include dielectric effects from carbonate bedrock and salt brines and/or scattering from sands. See “RFI mitigation” for information on 18.7 GHz RFI.

**mv:** The soil moisture data have been compared to WMO daily surface station summary of the day precipitation for the Northern Hemisphere and TRMM data. Correlation with station precipitation is typically between 0.2-0.8 with antecedent precipitation for areas where 18.7 GHz vegetation optical depth ( $-\log(tc)$ ) < 1.2 and open water fraction < 0.5. Note that AMSR-E  $f_w$  can be greater than MODIS open water mask because of seasonally varying flooding and saturated soils. Users are encouraged to create their own mask using the  $tc$  and  $f_w$  data provided using these thresholds. Intense wetting events that saturate the soil can cause soil moisture to rise significantly above the soil porosity, which is typically  $\approx 0.5$  for a loam soil. Soil moisture values greater than unity are set to unity. See “RFI mitigation” for information on 10.7 and 6.9 GHz RFI.

**V:** The integrated atmospheric water vapor data have been compared to MERRA re-analysis for selected locations spanning global landcover types ( $R=0.76$ ;  $RMSE = 6.3$  mm;  $Bias = 3.2$  mm). The retrievals are poorly conditioned for dense vegetation (boreal and tropical forests) resulting in noisy estimates. More extensive validation is in progress with other vertically integrated water vapor products (radiosondes and GPS occultation datasets).



**tc:** The vegetation opacity data have been compared to MODIS LAI, EVI, and NDVI (Jones et al. 2011). Preliminary research shows good correspondence (correlations up to 0.9), particularly for grassland and cropland locations. Areas with seasonally varying  $fw$  and strongly vertically oriented vegetation (e.g. reed lakes of the Okavango Delta, Botswana) show a drop in  $-\log(tc)$  during the wet season. This causes negative correlation with MODIS vegetation indices and is likely caused by radiometric (scattering by reeds), rather than actual biophysical factors. Other areas with more randomly oriented vegetation (temperate and high latitude swamps and bogs) do not show such an interaction between  $fw$  and  $-\log(tc)$ .

**fw and fwsm:** The open water fraction data have been compared to open water and irrigated area products from MODIS and JERS-1 and show good qualitative spatial agreement. However,  $fw$  can be greater than MODIS open water because of seasonally varying flooding and saturated soils. Carbonate rocks and scattering sands in the Sahara and Arabian deserts can cause widespread erroneous  $fw$  features in these areas. This is because the dielectric of carbonate rocks is higher than that of quartz, which was assumed in the algorithm. Additionally, sands can lower the effective emissivity by volume scattering. In contrast to adjacent areas where irrigation and open water actually occurs, such as along the Nile, Tigris, and Euphrates Rivers, carbonate deposits and sands show a time-stable  $fw$  signal. In other regions, dense vegetation canopies may mask underlying open water, such as along tributaries of the Amazon River, leading to lower than expected  $fw$ .

## IX. Additional Methods

The following section includes RFI mitigation and coastal snow/ice detection methods not discussed in Jones *et al.* [2009; 2010].

### **RFI mitigation:**

Soil moisture is calculated separately using 6.9 GHz and 10.7 GHz H-polarized brightness temperatures to mitigate RFI. The values obtained for 10.7 GHz are substituted where 6.9 GHz is affected by RFI according to our pre-screening flags; otherwise the 6.9 GHz channel is exclusively used.

RFI in AMSR-E 18.7 GHz observations has been documented to impact AMSR-E and WindSat ocean observations along the coastlines of the continental US after the September, 2007 launch of Direct-TV-10 in geostationary orbit over the continental US (see [www.ssmi.com/rfi](http://www.ssmi.com/rfi) for additional information). Glint from the reflected broadcast signal apparently impacts land observations along the northeastern coast of the US (particularly from New Jersey to Massachusetts) and also along the western shores of Lake Superior (near Duluth, Minnesota).

The problem is limited to Aqua's descending orbit. Other continental US areas may be affected where the glint angle is favorable to interference, but we have not yet documented other instances. Additional 18.7 GHz H-polarized RFI has been observed from a direct source in the northeastern US beginning in 2003; however, only two days (descending orbit August 19, 2003, and ascending orbit July 29, 2003) have been documented so far. AMSR-E 18.7 GHz H-polarized land RFI is screened as follows:

$$a = \frac{\epsilon_{23H,land} - \epsilon_{23H,water}}{\epsilon_{18H,land} - \epsilon_{18H,water}}$$

$$b = (\epsilon_{23H,water} - a * \epsilon_{18H,water}) * 255.0$$

$$\widehat{Tb}_{23H} = a * Tb_{18H} + b$$

$$dp = Tb_{18V} - Tb_{18H}$$

The equation for the line can be calculated using two emissivity endpoints, one for open water  $\epsilon_{(f,p),water}$  and the other for vegetated land  $\epsilon_{(f,p),land}$ , where  $f$  and  $p$  are the respective frequency and polarization. RFI in the 18.7 GHz H-polarized  $Tb$  is flagged if the following is true:

$$(Tb_{23H} < \widehat{Tb}_{23H}) \mid (dp < 0)$$

NOTE: These criteria occasionally flag areas adjacent to snow covered areas and active precipitation not captured by the snow and precipitation flags, although 18.7 GHz RFI has only been confirmed over the continental US. However, the flags were applied globally across the entire 2002-2008 (both D and A overpass) to keep the dataset consistent.

### **Snow and ice detection in regions with open water:**

An external freeze-thaw classification (Kim et al. 2011) derived using AMSR-E 36 GHz V-pol.  $Tb$  timeseries was employed to screen for frozen conditions. However, this classification does not adequately screen snow cover along coasts and sub-grid scale glaciers, and permanent ice fields impacting temperature retrievals. Therefore an additional classification using the 23.8 GHz and 18.7 GHz V-polarized  $Tb$  is employed to determine snow and ice in regions with open water. A scatter plot of the two frequencies reveals a triangular shaped lobe with pixels containing snow and ice (Comiso *et al.* 2003). The remaining pixels with a mixture of open water and snow- and ice- free land and fall along a single line. The equation for the line can be calculated using two emissivity endpoints one for open water  $\epsilon_{(f,p),water}$  and the other for vegetated land  $\epsilon_{(f,p),land}$ , where  $f$  and  $p$  are the respective frequency and polarization:

$$a = \frac{\varepsilon_{23V,land} - \varepsilon_{23V,water}}{\varepsilon_{18V,land} - \varepsilon_{18V,water}}$$

$$b = (\varepsilon_{23V,water} - a * \varepsilon_{18V,water}) * 273.15$$

$$\widehat{Tb}_{23V} = a * Tb_{18V} + b$$

Points falling below the line  $\widehat{Tb}_{23V}$  represent pixels containing ice and snow. Desert sands have a scattering signature similar to snow which requires an additional constraint to avoid flagging desert regions Grody [1988]. Ice and snow are flagged if the following is true:

$$(Tb_{23V} < \widehat{Tb}_{23V}) \ \& \ (Tb_{36V} < 250 \text{ K})$$

## X. Version and Update List

Version Number	Date	Summary
1.1	1/21/2010	Original data release
1.2	9/12/2011	Grid and flag updates
1.2 Update 1	4/23/2012	Data processed through the end of the AMSR-E record

### Details of changes in each version:

#### Version 1.1, Date: 1-21-2010

- Original data release.

#### Version 1.2, Date: 9-12-2011

- Land-water mask updated to correct a gridding error. The new data will be shifted south and east by one EASE grid-cell relative to the previous version. The new data vectors now contain 209091 elements (previously 209087).
- A new flag was added for when RFI is detected in both 6.9 and 10.7 GHz channels. Previously, such a situation resulted in a flag indicating “6.9 GHz RFI,” but gave no information on whether RFI was also detected for 10.7 GHz. This affects soil moisture retrievals because retrievals are possible when 6.9 GHz is affected by RFI, but 10.7 GHz is not, but are not possible when both channels are affected. Previous soil moisture data had missing retrievals for which there was not a coincident flag explaining the reason for the missing values.

- A new grid cell-wise frozen land surface flag was added based on an external freeze thaw classification of AMSR-E 36V GHz AM and PM overpass Tb series using algorithms from Kim et al. (2011). A cell is classified as frozen if both AM and PM Tb series are classified as frozen.

**Version 1.2, Update 1, Date: 4-23-2012**

- Data were processed through the end of the AMSR-E record (September 27, 2011). No other changes were made to algorithm code at this time. The AMSR-E instrument ceased operation on October 4, 2011.

## **XI. References**

**Please use the following references to cite these data:**

Jones, L.A., and J.S. Kimball, 2011. Daily Global Land Surface Parameters Derived from AMSR-E. Boulder Colorado USA: National Snow and Ice Data Center. Digital media (<http://nsidc.org/data/nsidc-0451.html>).

Jones, L. A., C. R. Ferguson, J. S. Kimball, K. Zhang, S. K. Chan, K. C. McDonald, E. G. Njoku, E. F. Wood. 2010 (in press). Daily land surface air temperature retrieval from AMSR-E: Comparison with AIRS/AMSU. *IEEE J. Appl. Earth Obs. Rem. Sens.*, Vol. 3, No. 1, pp. 111-23.

Jones, L. A., J. S. Kimball, E. Podest, K. C. McDonald, S. K. Chan, E. G. Njoku. 2009. A method for deriving land surface moisture, vegetation, and open water fraction from AMSR-E. *Proc. IEEE Int. Geosci. Rem. Sens. Symp. (IGARRS '09)*, July 13-17, Cape Town, South Africa. DOI:10.1109/IGARSS.2009.5417921.

**These references discuss dataset evaluation:**

Jones, M. O., L. A. Jones, J. S. Kimball, K. C. McDonald. 2011. Satellite passive microwave remote sensing for monitoring global land surface phenology. *Rem. Sens. Environ.*, Vol. 115, pp. 1102-1104.

Yi, Y. Y., J. S. Kimball, L. A. Jones, R. H. Reichle, K. C. McDonald. 2011. Evaluation of MERRA land surface estimates in preparation for the Soil Moisture Active-Passive Mission. *J. Clim.*, Vol. 24, pp. 3797- 3816.

**These references were used for developing pre-screening flags:**

- Comiso, J.C., D. J. Cavalieri, T. Markus. 2003. Sea ice concentration, ice temperature, and snow depth using AMSR-E Data. *IEEE Trans. Geosci. Rem. Sens.*, vol. 41, No. 2, pp. 243-252.
- Grody, N. C. 1988. Surface identification using satellite microwave radiometers. *IEEE Trans. Geosci. Rem. Sens.* , Vol. 26, pp. 850-859.
- Kim, Y., J. S. Kimball, K. C. McDonald, J. Glassy. 2011. Developing a Global Record of Daily Landscape Freeze/Thaw Status Using Satellite Passive Microwave Remote Sensing. *IEEE Trans. Geosci. Rem. Sens.*, Vol. 49, No. 3, pp. 949-960.
- McDonald, K. C., J. S. Kimball. 2005. Chapter 53: Freeze-thaw states using both active and passive microwave sensors. In *Encyclopedia of Hydrological Sciences*, M. G. Anderson, (Ed.); John Wiley and Sons, Hoboken, N.J., pp. 1-15.
- Njoku, E. G., P. Ashcroft, T. K. Chan, L. Li. 2005. Global survey and statistics of radio-frequency interference in AMSR-E land observations. *IEEE Trans. Geosci. Rem. Sens.*, Vol. 43, No. 5, pp. 938-947.

**These references describe AMSR-E input data used for parameter retrievals:**

**AE\_L2A data:**

- Ashcroft, P., F. Wentz. 1999. Algorithm Theoretical Basis Document, AMSR level 2A algorithm,” *RSS Tech. Report 121 599B-1*. Santa Rosa, CA.

**EASE-Grid data:**

- Knowles, K. W., M. H. Savoie, R. L. Armstrong, and M. J. Brodzik. 2006, updated 2011. [AMSR-E/Aqua Daily EASE-Grid Brightness Temperatures](#), [June 19, 2002 to Sept. 27, 2011]. Boulder, Colorado USA: National Snow and Ice Data Center. Digital media. Downloaded: 4/18/2012.